# Charge and Magnetic Order in $La_{0.5}Sr_{1.5}MnO_4$

B. J. Sternlieb, J. P. Hill, and U. C. Wildgruber
*Physics Department, Brookhaven National Laboratory, Upton, New York 11973*

G. M. Luke and B. Nachumi
*Department of Physics, Columbia University, 538 W. 120th Street, New York, New York 10027*

Y. Moritomo and Y. Tokura
*Joint Research Center for Atom Technology, Tsukuba, Ibaraki 305, Japan*
(Received 24 July 1995)

Elastic neutron scattering measurements characterizing the charge and magnetic order in $La_{0.5}Sr_{1.5}MnO_4$ are presented. Superlattice reflections corresponding to an alternating $Mn^{+3}/Mn^{+4}$ pattern with wave vector $\mathbf{q}_{co} = (\frac{1}{2}, \frac{1}{2}, 0)$ are observed below the charge ordering temperature, $T_{co} \approx 217$ K. Below the Néel temperature, $T_N \approx 110$ K, the magnetic moments associated with these ions form an ordered structure with dimensions $2\sqrt{2}\,a \times 2\sqrt{2}\,a \times 2c$ relative to the underlying chemical cell.

PACS numbers: 75.30.Fv, 75.40.Gb

Why is the superconducting transition temperature in the prototypical high-$T_c$ superconductor $La_{2-x}Ba_xCuO_4$ sharply reduced when $x = \frac{1}{8}$? Measurements by Tranquada *et al.* [1] on $La_{2-x-0.4}Nd_{0.4}Sr_xCuO_4$ with $x \approx \frac{1}{8}$ indicate that this suppression results from the real-space separation of holes and spins into an ordered phase consisting of antiferromagnetic "stripes" separated by antiphase, hole-rich domain walls. This order is surprisingly similar to that observed in the hole doped nickelates [2,3] $La_{2-x}Sr_xNiO_4$ and $La_2NiO_{4+\delta}$. Studies of the isostructural manganate $La_{1-x}Sr_{1+x}MnO_4$ are clearly needed for a general understanding of charge and spin separation in the layered transition metal oxides, and, in particular, to elucidate the role played by striping in the superconducting cuprates [4]. In addition, experiments on $La_{1-x}Sr_{1+x}MnO_4$ should shed light on the physics of the related cubic perovskite $La_{1-x}Sr_xMnO_3$. The contrast between these two strongly correlated systems at comparable doping levels is sharp; the former exhibits an insulating character [5,6], while the latter is metallic with a large, giant magnetoresistance [7,8].

In this Letter we present structural and magnetic neutron scattering data describing charge and spin order in single crystal $La_{0.5}Sr_{1.5}MnO_4$. Our measurements demonstrate that the formal $Mn^{+3.5}$ valence of this compound orders, below a charge ordering temperature, $T_{co} \sim 217$ K, in an alternating $Mn^{+3}/Mn^{+4}$ pattern as first suggested by the electron diffraction work of Moritomo *et al.* [6]. The resulting charge ordered unit cell has dimensions $\sqrt{2}a \times \sqrt{2}a \times c$. These neutron results, together with x-ray and electron microphobe data on the same sample, also explain earlier discrepancies regarding the fundamental wave vector of the charge order in this system [6,9]. Below the Néel temperature, $T_N \sim 110$ K, the moments associated with the manganese ions form a magnetically ordered structure with a $2\sqrt{2}a \times 2\sqrt{2}a \times 2c$ unit cell. A detailed magnetic model, which accounts for the observed neutron scattering data, is derived from the spin structure originally proposed by Goodenough [10] for the $MnO_2$ layers of the cubic perovskite $La_{0.5}M(II)_{0.5}MnO_3$.

The approximately cylindrical ($\phi$ : 4 mm $\times$ $l$ : 25 mm) crystal used for these measurements has been extensively characterized [6]. At room temperature, the crystal space group is $I4/mmm$ with tetragonal lattice constants $a = 3.86$ Å and $c = 12.44$ Å [11]. The sample FWHM mosaic is 1.35°. The crystal was mounted in a closed cycle $^4$He refrigerator in successive orientations allowing momentum transfers with indices $q = (h, h, l)$, $(h, 0, l)$, $(h, k, 0)$, and $(3h, h, l)$.

Determining the magnetic or structural origin of superlattice reflections is straightforward as the $\mathbf{q}$ dependences of the associated intensities differ markedly. For both cases, the elastic neutron scattering cross section has the form $d\sigma_{n,m}/d\Omega(\mathbf{q}) \propto \sum_{\boldsymbol{\tau}_{n,m}} |F_{n,m}(\mathbf{q})|^2 \delta(\mathbf{q} - \boldsymbol{\tau}_{n,m})$, where the sum extends over all nuclear (magnetic) reciprocal lattice vectors. For small atomic displacements, $\mathbf{r}_j = \mathbf{r}_j^0 + \boldsymbol{\epsilon}_j$, the nuclear structure factor $F_n(\mathbf{q})$ can be written as

$$F_n(\mathbf{q}) \propto \sum_{j \in \substack{\text{structural} \\ \text{cell}}} b_j\{1 + i\mathbf{q} \cdot \boldsymbol{\epsilon}_j\} e^{i\mathbf{q}\cdot\mathbf{r}_j^0} e^{-W_j}, \qquad (1)$$

where $b_j$ is the nuclear scattering length and $e^{-W_j}$ is the Debye-Waller factor. This results in a $\sim|\mathbf{q} \cdot \boldsymbol{\epsilon}|^2$ momentum dependence for structural superlattice intensities. The magnetic structure factor can be written as

$$\mathbf{F}_m(\mathbf{q}) \propto \sum_{j \in \substack{\text{magnetic} \\ \text{cell}}} \{\hat{\mathbf{q}} \times \langle \mathbf{S}_j \rangle \times \hat{\mathbf{q}}\} f(\mathbf{q}) e^{i\mathbf{q}\cdot\mathbf{r}_j} e^{-W_j}, \quad (2)$$

where $\mathbf{S}_j$ is the spin at site $j$. The magnetic form factor $f(\mathbf{q})$ accounts for the spatial distribution of unpaired electron spins and leads to a falloff of intensities at

  

large $|\mathbf{q}|$. The vector product in Eq. (2) also results in a distinctive magnetic signature.

The nuclear ($\odot$) and additional structural ($\circ$) and magnetic ($\bullet$) superlattice peaks observed with $\mathbf{q} = (h, h, l)$ at $T = 9$ K are shown schematically in the inset to Fig. 1. The high temperature, body-centered structure of this system permits nuclear reflections with indices $q = \{(h, k, l)|h + k + l = 2n\}$. Low temperature measurements of these reflections reveal no evidence of nuclear peak splitting, or a breaking of tetragonal symmetry. Scans through the structural superlattice peaks along $\mathbf{q} = (\frac{3}{2}, \frac{3}{2}, l)$ and $\mathbf{q} = (\frac{1}{2}, \frac{1}{2}, l)$ [dashed lines 1(a) and 1(b) in inset] are shown in the main panels of Fig. 1. The range of the $(\frac{1}{2}, \frac{1}{2}, l)$ data is limited by contamination from $La_{1-x}Sr_{2+x}Mn_2O_7$ intergrowths. This impurity, which is distinguished by a $c = 20.07$ Å lattice parameter, accounts for less than $\sim$0.6% of the Mn sites in the sample. The weak $l$ dependence of the integral peak intensities in both these spectra and the strong dependence of the intensities on in-plane momentum transfer demonstrate that this scattering is due to a structural deformation with displacements, $\boldsymbol{\epsilon}$, that lie primarily in the $MnO_2$ plane. Simultaneous resolution corrected fits to both spectra, using a sum of equal amplitude Lorentzians,

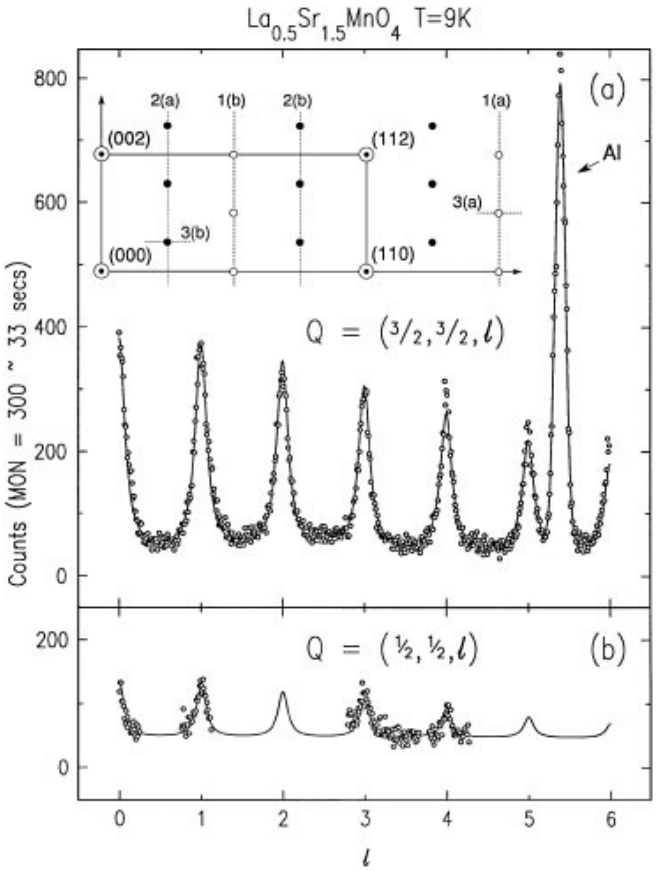


FIG. 1. Structural scattering along (a) $\mathbf{q} = (\frac{3}{2}, \frac{3}{2}, l)$ and (b) $\mathbf{q} = (\frac{1}{2}, \frac{1}{2}, l)$. Inset: The $\mathbf{q} = (hhl)$ scattering plane. Nuclear reflections are allowed at $h + k + l = 2n$. Light (dark) circles are structural (magnetic) peaks.

centered at integral $l$ and scaled by the structural $|\mathbf{q} \cdot \boldsymbol{\epsilon}|^2$ dependence of Eq. (1), are shown in the figure. The fit quality ($\chi^2 = 1.7$) indicates that the decrease in peak intensities at high $l$ in the raw data is entirely due to the $|\mathbf{q}|$ dependence of the instrument resolution function. Normal to the $MnO_2$ planes, the charge correlation length is $\xi_c^{co} = 50$ Å or $\sim$8 $MnO_2$ layers. In contrast, the in-plane correlation length, measured along $(h, h, 1)$, is resolution limited: $\xi_{ab}^{co} \gtrsim 300$ Å.

These superlattice reflections, together with the structural peaks seen in other crystal orientations, are cataloged in Table I. A simple planar oxygen breathing-mode distortion, in which the oxygen between nearest neighbor Mn atoms moves towards the higher valence $Mn^{+4}$ ion, is consistent with this scattering. The resulting "charge-ordered" phase has a metrically nearly tetragonal, orthorhombic *Cmmm* space group and a $\sqrt{2}a \times \sqrt{2}a \times c$ unit cell as shown in Fig. 2. The intensities of the $(hhl)$ superlattice reflections, which are the strongest associated with this breathing mode, indicate a fractional change in the Mn-O bond length of $\sim$1%.

In contrast to these results, earlier electron diffraction studies by Moritomo *et al.* [6] on the same crystal reported evidence of $(\frac{1}{4}, \frac{1}{4}, 0)$ and $(\frac{3}{4}, \frac{3}{4}, 0)$ structural scattering as well as scattering at $(\frac{1}{2}, \frac{1}{2}, 0)$, while the electron diffraction results of Bao *et al.* [9] on a sample with the same nominal stoichiometry report scattering principally at $(\frac{1}{4}, \frac{1}{4}, 0)$ and $(\frac{3}{4}, \frac{3}{4}, 0)$ with only limited intensity at $(\frac{1}{2}, \frac{1}{2}, 0)$. To address these discrepancies, x-ray measurements were performed on the same crystal used in the neutron work at the X22C beam line of the National Synchrotron Light Source. At $T = 10$ K, scattering was observed at $(\frac{1}{4}, \frac{1}{4}, l = 6, 8, 10)$ for $5.5 \leq l \leq 10.5$, in addition to superlattice reflections at $(\frac{1}{2}, \frac{1}{2}, l)$, in apparent disagreement with the neutron results. These additional x-ray satellites possess roughly the same temperature dependence as the $(\frac{1}{2}, \frac{1}{2}, l)$ superlattice peaks. At $T = 130$ K, additional measurements along $(\frac{3}{4}, \frac{3}{4}, l)$ between

TABLE I. Observed reflections $\{m, n \in \text{integers}\}$. Magnetic reflections along $(h, 0, l)$ are due to the $Mn^{+4}$ spins. The $(h, h, l)$ and $(3h, h, l)$ reflections are due to the $Mn^{+3}$ spins.

| **q** | Structural | 3D Magnetic[a] |
|---|---|---|
| $(h, k, 0)$ | $h = \frac{2n+1}{2}$, $k = \frac{2m+1}{2}$ | None |
| $(h, 0, l)$ | None | $h = \frac{2n+1}{2}$, $l = \frac{2m+1}{2}$ |
| $(h, h, l)$ | $h = \frac{2n+1}{2}$, $l = m$ | $h = \frac{2n+1}{4}$, $l = \frac{2m+1}{2}$ |
| | | $(h = \frac{2n+1}{4}, l = 2m)$[b] |
| $(3h, h, l)$ | $h = \frac{2n+1}{2}$, $l = m$ | $h = \frac{2n+1}{4}$, $l = \frac{2m+1}{2}$ |
| | | $(h = \frac{2n+1}{4}, l = 2m + 1)$[b] |

[a]2D, rodlike magnetic scattering is clearly visible in all zones as well.

[b]Reflections corresponding to the minority $MnO_2$ plane stacking vector (see Fig. 2).

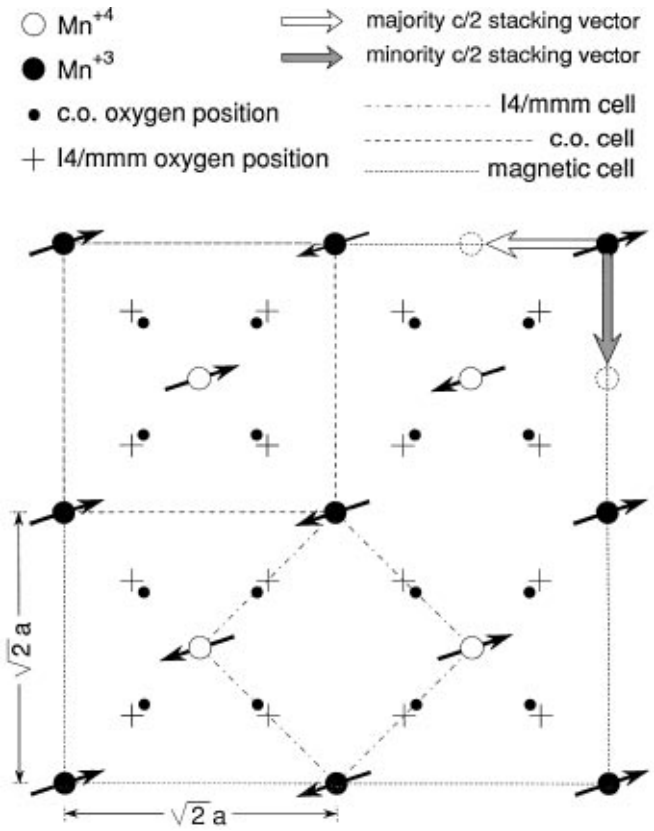


FIG. 2. The $MnO_2$ spin configuration originally proposed by Goodenough [10]. The majority and minority magnetic reflections described in the text result from the translation of successive $MnO_2$ planes by the stacking vectors shown in the figure.

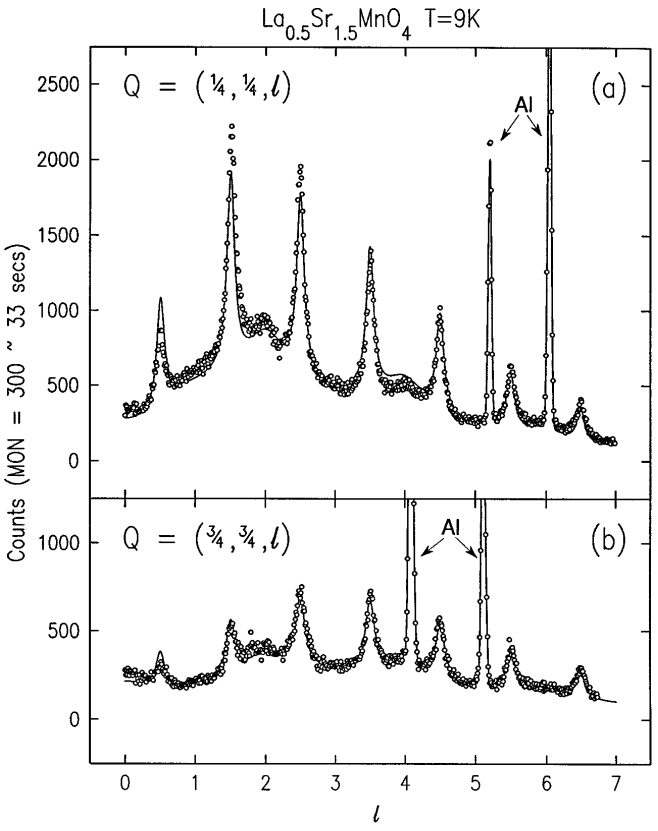


FIG. 3. Magnetic data: (a) $\mathbf{q} = (\frac{1}{4}, \frac{1}{4}, l)$ and (b) $\mathbf{q} = (\frac{3}{4}, \frac{3}{4}, l)$. The half-integral $l$ peaks result from the majority stacking shown in Fig. 2, while the even integer $l$ peaks are due to the minority stacking. The broad, weakly $l$ dependent intensity in both spectra indicates a strong 2D contribution to the total signal.

$7.75 \leq l \leq 11.25$ also resulted in a peak at $l = 8$, though no scattering above background was observed for $l = 9$, 10, or 11. Subsequent high statistics neutron scattering measurements along $(\frac{3}{4}, \frac{3}{4}, l)$ over $0 \leq l \leq 11.25$ at the same temperature observed this isolated, $l = 8$, peak but no other peaks at smaller $l$, suggesting that this peak has a spurious origin. Scans along $(\frac{1}{4}, \frac{1}{4}, l)$ also show no evidence of the superlattice scattering observed in the x-ray measurements. Electron microphobe analysis suggests that this inconsistency is due to excess oxygen and variations in the La/Sr ratio at the crystal surface. As the surface is preferentially sampled by the x-ray and electron diffraction measurements, an alternate charge dressing near the crystal surface could produce additional reflections. In contrast, neutrons probe the entire crystal and are largely insensitive to these surface properties.

Scans of the magnetic scattering along $\mathbf{q} = (\frac{1}{4}, \frac{1}{4}, l)$ and $\mathbf{q} = (\frac{3}{4}, \frac{3}{4}, l)$ [dashed lines 2(a) and 2(b) in Fig. 1, inset] are shown in Fig. 3. Three sources of scattering can be distinguished: well ordered scattering at half integer $l$, small additional peaks centered about even $l$, and substantial two-dimensional (2D) scattering broadly distributed along $l$. The presence of $(\frac{1}{4}, \frac{1}{4}, \frac{2n+1}{2})$ peaks in these spectra indicates that the magnetic unit cell has dimensions $2\sqrt{2}a \times 2\sqrt{2}a \times 2c$ relative to the $I4/mmm$ cell. The $MnO_2$ spin model shown in Fig. 2, originally proposed by Goodenough [10] for the cubic perovskite $La_{0.5}M(II)_{0.5}MnO_3$, agrees well with our half-integer $l$ data if the stacking of successive $MnO_2$ planes is offset by the "majority" stacking vector shown in the figure. The weak reflections at even $l$ in the magnetic $(h, h, l)$ data and at odd $l$ in the magnetic $(3h, h, l)$ data (not shown) arise from an alternate, "minority" stacking of these layers. Either stacking arrangement results in the same allowed structural reflections. The $(h0l)$ magnetic reflections are also the same for both choices of stacking vector. A notable feature of this model is the fact that the magnetic intensities observed for $\mathbf{q} = (h, h, l)$ are exclusively due to the $Mn^{+3}$ moments, while the $\mathbf{q} = (h, 0, l)$ scattering results solely from the ordered $Mn^{+4}$ moments.

The magnetic intensities in both panels of Fig. 3 initially increase with increasing $l$. This suggests that the spins responsible for this scattering lie primarily in the basal plane so that the vector product of Eq. (2) results in an intensity that varies as

$$\sin^2\phi_s + \cos^2\phi_s \sin^2\theta\,, \qquad (3)$$

where $\theta$ is the angle the scattering vector makes with the $MnO_2$ plane and $\phi_s$ is the angle between the spins and the $(h, h, 0)$ axis. The attenuation at large $l$ is due to the

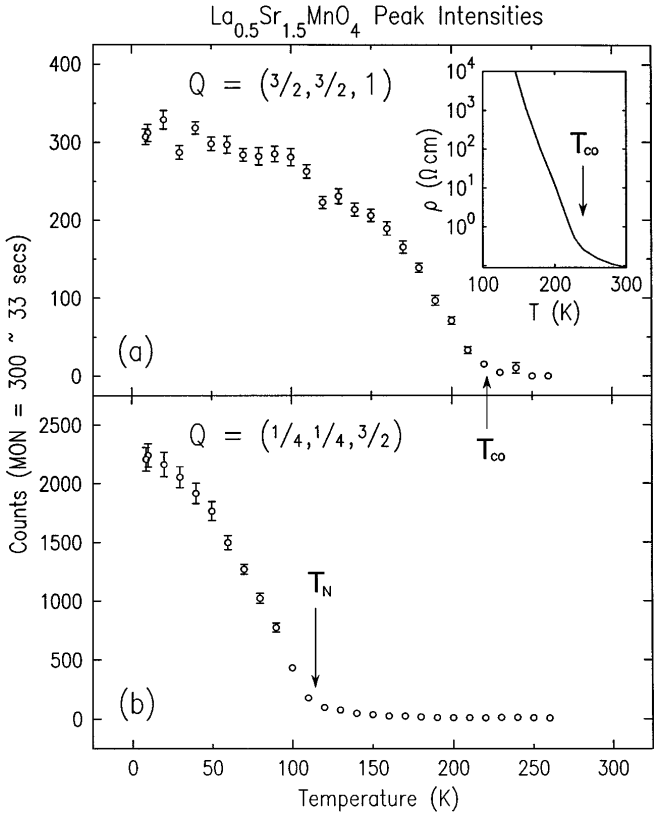


FIG. 4. Temperature dependence of the (a) charge and (b) magnetic order. Inset in (a): Resistivity vs $T$.

magnetic form factor. The fits shown in the figure employ two sets of Lorentzian line shapes of *constant* amplitude and width, one set centered at half-integral $l$ (majority stacking) and one set at even integer $l$ (minority stacking), as well as an $l$ independent signal to account for the 2D scattering. These are then multiplied by a generic Mn form factor and convoluted with the instrument resolution. The reasonable quality of these fits indicates that the $l$ dependences and relative intensities of the two spectra are entirely attributable to the angular dependence of Eq. (3) and the $|\mathbf{q}|$ dependence of the magnetic form factor. The width of the majority peaks implies a magnetic correlation length normal to the $MnO_2$ planes of $\xi_c^{\mathrm{maj\,mag}} = 33$ Å, while the widths of the broad minority stacking peaks at even $l$ result in a characteristic length, $\xi_c^{\mathrm{min\,mag}} = 6$ Å, which is roughly equal to the separation between $MnO_2$ planes. As in the structural data, measurements along $(h, h, \frac{3}{2})$ indicate that the magnetic, in-plane correlation length is resolution limited ($\xi_{ab}^{\mathrm{mag}} \gtrsim 300$ Å). The fit value of $\phi_s$ suggests that the $Mn^{+3}$ spins lie along the $(2, 1, 0)$ direction. This orientation is also consistent with our $(3h, h, l)$ magnetic data. The relative size of the moments associated with the two manganese species, deduced from the $(hhl)$ and $(hk0)$ magnetic intensities, is roughly $S(Mn^{+3})/S(Mn^{+4}) = 1.2 \pm 0.1$, slightly smaller than the nominal $4/3$ value. Determination of the absolute moment associated with the Mn ions is difficult due to the complexity of the observed magnetic scattering. However, the ratio of the observed magnetic $(\frac{1}{4}, \frac{1}{4}, \frac{3}{2})$ and nuclear $(0, 0, 2)$ intensities suggests a lower bound for the $Mn^{+3}$ spin of $S \gtrsim 1.6$.

The temperature dependence of the $\mathbf{q} = (\frac{3}{2}, \frac{3}{2}, 1)$ structural superlattice peak intensity is shown in Fig. 4(a). The charge ordering temperature, $T_{\mathrm{co}} \sim 217$ K, is the same temperature below which this crystal reveals a sharp increase in resistivity [6] [Fig. 4(a), inset] as is consistent with the localized character of the ordered charge. The temperature dependence of the $\mathbf{q} = (\frac{1}{4}, \frac{1}{4}, \frac{3}{2})$ magnetic superlattice reflection is shown in Fig. 4(b). The Néel temperature $T_N \sim 110$ K associated with these data agrees with earlier susceptibility measurements on this crystal [6]. Evidence of 2D magnetic scattering in the $MnO_2$ planes between the charge and magnetic ordering temperatures was also observed.

The data presented here demonstrate that $La_{0.5}Sr_{1.5}MnO_4$ has charge and magnetic ordering transitions at $T_{\mathrm{co}} \sim 217$ K and $T_N \sim 110$ K, respectively. The low-temperature magnetic data are well described by extensions to Goodenough's original cubic perovskite model [10]. In contrast, the charge order observed in these neutron scattering measurements, in which no evidence of $(\frac{1}{4}, \frac{1}{4}, l)$ scattering has been seen, seems to possess a much simpler structure than earlier measurements [6,9] and theory [10] would suggest. Our neutron data are most simply described in terms of a planar oxygen breathing mode model as described above. Measurements of the dynamics associated with the charge and magnetic phases are currently underway. Efforts to extend these measurements to samples with different La/Sr stoichiometries are also planned.

We wish to thank J. M. Tranquada, J. D. Axe, G. Shirane, D. E. Cox, and J. B. Goodenough for various conversations. Work at Brookhaven National Laboratory was carried out under Contract No. DE-AC0276CH00016, Division of Materials Science, U.S. Department of Energy. Support was also received from the New Energy and Industrial Technology Development Organization (NEDO), Japan.

[1] J. M. Tranquada *et al.*, Nature (London) **375**, 561 (1995).
[2] J. M. Tranquada, J. E. Lorenzo, D. J. Buttrey, and V. Sachan, Phys. Rev. B **52**, 3581 (1995).
[3] V. Sachan *et al.*, Phys. Rev. B **51**, 12 742 (1995).
[4] V. J. Emery and S. A. Kivelson, Physica (Amsterdam) **235–240C**, 189 (1994).
[5] R. A. M. Ram, R. Ganguly, and C. N. R. Rao, J. Solid State Chem. **70**, 82 (1987).
[6] Y. Moritomo *et al.*, Phys. Rev. B **51**, 3297 (1995).
[7] Y. Tomioka *et al.*, J. Phys. Soc. Jpn. **63**, 3931 (1994).
[8] A. Urushibara *et al.*, Phys. Rev. B **51**, 14 103 (1995).
[9] W. Bao, S. A. Carter, C. H. Chen, and S.-W. Cheong (unpublished).
[10] J. B. Goodenough, Phys. Rev. **100**, 564 (1955).
[11] J. C. Bouloux, J. L. Soubeyroux, A. Daoudi, and G. L. Flem, Mater. Res. Bull. **16**, 855 (1981).